Phosphorylated Phospholamban Stabilizes a Compact Conformation of the Cardiac Calcium-ATPase

Sandeep Pallikkuth,[†] Daniel J. Blackwell,[†] Zhihong Hu,[†] Zhanjia Hou,[†] Dane T. Zieman,[†] Bengt Svensson,[‡] David D. Thomas,[‡] and Seth L. Robia[†*]

[†]Department of Cell and Molecular Physiology, Loyola University Chicago, Maywood, Illinois; and [‡]Department of Biochemistry, Molecular Biology, and Biophysics, University of Minnesota, Minneapolis, Minnesota

ABSTRACT   The sarcoendoplasmic reticulum calcium ATPase (SERCA) plays a key role in cardiac calcium handling and is considered a high-value target for the treatment of heart failure. SERCA undergoes conformational changes as it harnesses the chemical energy of ATP for active transport. X-ray crystallography has provided insight into SERCA structural substates, but it is not known how well these static snapshots describe in vivo conformational dynamics. The goals of this work were to quantify the direction and magnitude of SERCA motions as the pump performs work in live cardiac myocytes, and to identify structural determinants of SERCA regulation by phospholamban. We measured intramolecular fluorescence resonance energy transfer (FRET) between fluorescent proteins fused to SERCA cytoplasmic domains. We detected four discrete structural substates for SERCA expressed in cardiac muscle cells. The relative populations of these discrete states oscillated with electrical pacing. Low FRET states were most populated in low Ca (diastole), and were indicative of an open, disordered structure for SERCA in the E2 (Ca-free) enzymatic substate. High FRET states increased with Ca (systole), suggesting rigidly closed conformations for the E1 (Ca-bound) enzymatic substates. Notably, a special compact E1 state was observed after treatment with β-adrenergic agonist or with coexpression of phosphomimetic mutants of phospholamban. The data suggest that SERCA calcium binding induces the pump to undergo a transition from an open, dynamic conformation to a closed, ordered structure. Phosphorylated phospholamban stabilizes a unique conformation of SERCA that is characterized by a compact architecture.

INTRODUCTION

The sarco(endo)plasmic reticulum Ca-ATPase (SERCA) is a P-type ion pump responsible for transporting Ca ions from the cytoplasm to sarcoendoplasmic reticulum (SR) in muscle cells. This process is critical during cardiac diastole (relaxation), because the muscle must relax to allow for adequate filling of the ventricles with blood. SERCA function is also important for systole (cardiac contraction), because it is solely responsible for creating the large store of SR Ca that is released to initiate activation of the muscle. Disordered SERCA expression (1), function (2), or regulation (3–5) are associated with heart disease, underscoring the central role of SERCA in cardiac physiology.

Biochemical and biophysical studies employing a variety of methods have provided insight into SERCA structure/function relationships. As examples, conformational changes of SERCA have been studied by quantification of spectroscopic changes (6) fluorescence anisotropy decay of an N-domain or P-domain-targeted probe (7), partial proteolysis (7,8), transient phosphorescence anisotropy (9), molecular dynamics simulations (10,11), or by quantifying the altered crosslinking of phospholamban (PLB) (or other regulators) with the pump (12–14). We and others have also quantified pump dynamics with intramolecular FRET between fluorescent labels attached to SERCA cytoplasmic domains (15–18). Collectively, these biochemical studies

have revealed that enzymatic transitions of the Ca transport cycle are accompanied by conformational changes between two broad classes of structures. These are the E1 (Ca-bound) and E2 (Ca-free) conformations, characterized by different relative positions of three cytoplasmic domains (N, A, and P), collectively known as the "cytoplasmic headpiece".

Moreover, a series of high-resolution structure solutions have elucidated SERCA enzymatic substates in atomic detail (reviewed in Moller et al. (19)), revealing how conformational changes in the headpiece are transmitted to the trans-membrane domain to alter the occlusion and affinity of the Ca binding sites. The first x-ray crystal structures of SERCA suggested that Ca induces a large increase in the separation of the N and A domains (20,21), but recent crystallography (22–24) and in vitro fluorescence resonance energy transfer (FRET) experiments (18) depict a closed cytoplasmic headpiece for Ca-bound SERCA, and suggest that the conformational change may be smaller than previously thought.

To investigate SERCA conformational changes in live cells, we previously utilized a two-color SERCA construct composed of SERCA2a fused to a Cerulean (Cer) FRET donor and a yellow fluorescent protein (YFP) FRET acceptor ((16) and S. J. Gruber, R. L. Cornea, J. Li, K. C. Peterson, T. M. Schaaf, G. D. Gillispie, R. Dahl, K. M. Zsebo, S. L. Robia, and D. D. Thomas, unpublished) (CY-SERCA, Fig. 1 A). Several variants of this intramolecular FRET sensor were characterized and shown to be functional with respect to subcellular localization, ATPase activity,

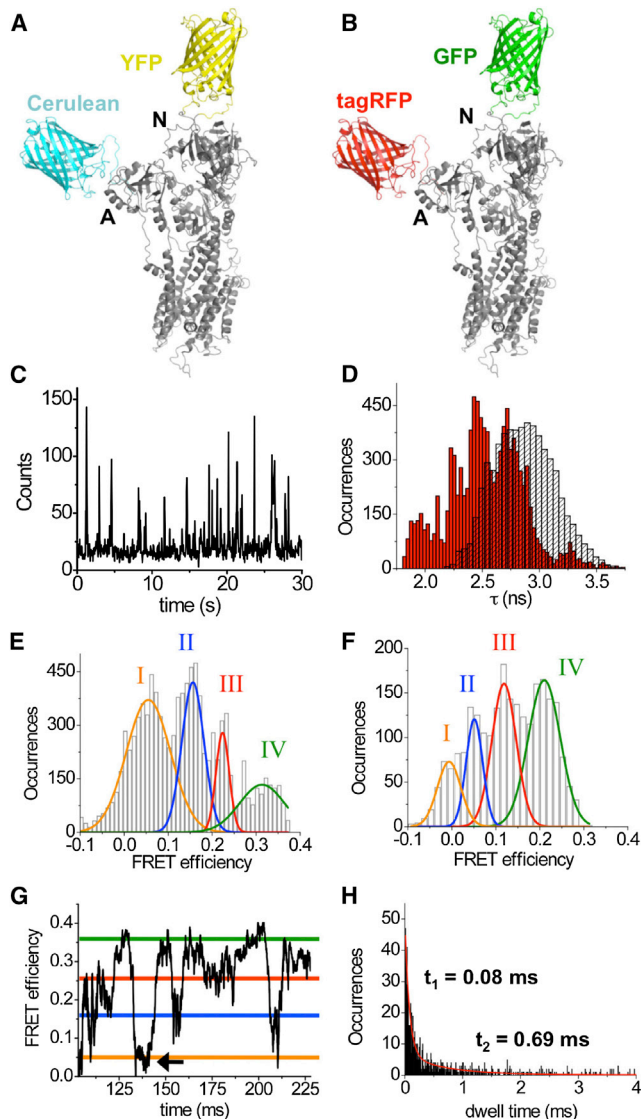http://dx.doi.org/10.1016/j.bpj.2013.08.045

CrossMark

FIGURE 1 Single molecule fluorescence spectroscopy of two-color SERCA. (A) CY-SERCA comprises a Cerulean FRET donor fused to the N-terminus of SERCA (*gray*) in the actuator, or A-domain, and an intrasequence YFP inserted in the nucleotide-binding, or N-domain [16]. (B) RG-SERCA is an analogous construct composed of a TagRFP acceptor fused to the N-terminus in the A-domain and GFP (*green*) donor inserted in the N-domain. Changes in SERCA conformation alter the distance between the N- and A-domains, changing intramolecular FRET efficiency. (C) Fluorescence bursts from single molecules of detergent-solubilized two-color SERCA. (D) Histogram of the fluorescence lifetime measurements obtained from two-color RG-SERCA (*red*) or control GFP-SERCA (*black*). (E) Histogram of FRET efficiency calculated from the lifetime measurements shown in panel D. Gaussian fit revealed subpopulations consistent with four discrete conformations of SERCA. (F) CY-SERCA also exhibited four discrete FRET states. The reduced FRET of these states (compared to panel E) was consistent with a shorter R_0 for the Cer-YFP FRET pair. (G) RG-SERCA single-molecule FRET time trajectory. (*Horizontal lines* indicate States I–IV (*orange* through *green*) identified by Gaussian analysis, as in panel E). The pump is observed to transiently sample the low FRET state (at *arrow*), before returning to higher FRET conformations, suggesting that State I does not represent denatured protein. (H) Analysis of dwell time for SERCA-sampling States I–IV revealed a biphasic distribution of dwell times characterized by fast (80 μs) and slow (690 μs) kinetics. To see this figure in color, go online.

Ca uptake activity, and regulation by phospholamban (PLB). The constructs also exhibited conformation-dependent FRET. In particular, a construct with the fluorescent proteins fused to the A- and N-domains showed decreased FRET with thapsigargin (Tg) and increased FRET with Ca. The data suggested that the donor-acceptor distance decreased with the E2-to-E1 conformational change, consistent with a closure of the SERCA cytoplasmic headpiece [16].

Here we extend this work with an improved two-color SERCA that benefits from a higher efficiency FRET pair (RG-SERCA, Fig. 1 B). We also used a quantitative spectroscopic method that resolves SERCA structural heterogeneity. The goal of these experiments was to identify discrete structural substates of SERCA and quantify the population of those states in live cells. In particular, we measured dynamic changes in the distribution of SERCA among several discrete conformations in electrically paced adult ventricular myocytes.

MATERIALS AND METHODS

Molecular biology and cell culture

The engineering and functional characterization of two-color SERCA was described in detail in Hou et al. [16]. For some of these experiments we used a rabbit SERCA2a construct (i.e., residue 509) described in Hou et al., which is labeled with Cerulean on the N-terminus and an EYFP intrasequence tag inserted before residue 509 on the SERCA nucleotide-binding domain. This Cer/YFP construct is referred to as "CY-SERCA" here. We also used an analogous construct, "RG-SERCA", in which the N-terminus was fused to TagRFP and EGFP was inserted as an intrasequence tag before residue 509 in the N-domain. The Cer-YFP pair has a Förster distance (R_0) of 49.8 Å and the GFP-TagRFP pair has an R_0 of 58.3 Å [26].

Expression of two-color SERCA in AAV-293 cells was performed as previously described in Hou et al. [16] and Kelly et al. [27]. Briefly, cells were transfected with plasmids encoding two-color SERCA using the MBS mammalian transfection kit (Agilent Technologies, Stratagene, La Jolla, CA). The transfected cells were trypsinized and replated onto poly-D-lysine-coated glass-bottom dishes and allowed to attach for 2–4 h before being used for measurements. Cotransfection of two-color SERCA with nonfluorescent S16A-PLB or S16E-PLB was performed at a plasmid/molar of 1:10.

For single-molecule experiments, the protein was solubilized in detergent as follows: 0.1% dodecylphosphocholine (Sigma-Aldrich, St. Louis, MO) in phosphate-buffered saline was gently layered over AAV-293 cells expressing two-color SERCA, and incubated at room temperature for 45 min and sonicated for 2 min. The solution was withdrawn and centrifuged at 16,000 g for 10 min, and the supernatant was transferred to a chambered coverglass (MatTek, Ashland, MA) for spectroscopy.

Adenoviral vectors of two-color SERCA were prepared using the AdEasy Adenoviral Vector System (Agilent Technologies, Santa Clara, CA). Adult cardiac ventricular myocytes were enzymatically isolated from adult New Zealand White rabbits [28]. All protocols were approved by the Loyola University Chicago Institutional Animal Care and Use Committee. Myocytes were transferred to culture vessels and washed with fresh PC-1 medium (Lonza, Basel, Switzerland). Two-color SERCA adenoviruses were added at a multiplicity of infection of 1000.

Cells were paced for 48 h in culture using a C-Pace EP pacer (IonOptix, Milton, MA) set to 10 volts with a frequency of 0.1 Hz and 5-ms pulse duration. Typically, 50% of cells were rod-shaped after 48 h in culture, and 80%

of those expressed detectable fluorescent protein. The percentage of fluorescent cells was not increased by a multiplicity of infection of 10,000. During spectroscopy experiments, electrical pacing of cardiac myocytes was performed with a stimulator (Grass S44; Astro-Med, West Warwick, RI), with 50-V stimulation, 5-ms duration, 0.25 Hz. The onset of contraction after a stimulus was detected as a motion deflection of fluorescence intensity. Data were integrated from multiple consecutive contraction/relaxation cycles, with systole measurements taken from a 800-ms interval beginning after the onset of contraction, and diastole measurements were taken from an 800-ms interval beginning 100 ms after contraction was complete.

Time-resolved fluorescence spectroscopy and imaging

Time-correlated single-photon counting (TCSPC) and fluorescence imaging were performed on an inverted confocal microscope (TCS-SP5; Leica Microsystems, Buffalo Grove, IL) equipped with a $63\times$ 1.20 NA water immersion objective (Leica Microsystems) and a pulsed Ti-Sapphire laser (Coherent, Bloomfield, CT), with excitation at 840 nm. Emission was split by a dichroic filter centered at 560 nm and passed through filters of 500–550 nm (for EGFP fluorescence) and 607–683 nm (for TagRFP fluorescence). Avalanche photo diodes (SPCM-AQRH; PerkinElmer, Waltham, MA) were used for detection of photons. The signals from the photo diodes passed to a pulse inverter (APPI-D; Becker & Hickl, Berlin, Germany) and 20-dB attenuator and a TCSPC router (HRT-41; Becker & Hickl) for simultaneous data collection of both emission channels. The signal output and the routing information from the router were transmitted to a TCSPC card (SPC-830; Becker & Hickl) to record temporal information for each detected photon. A synchronization reference signal for the TCSPC measurements was obtained by directing a portion of the excitation laser onto a photodiode (PHD-400-N; Becker & Hickl).

Temporal information was recorded as two different time tags for each detected photon: t_1, the microscopic arrival time relative to the previously measured synchronization reference signal, and t_2, indicating the macroscopic arrival time of the photon measured with respect to the start of the experiment. Time tag t_1 provides information about the nanosecond-scale fluorescence lifetime and t_2 measures the timecourse of the experiment with millisecond time resolution. TCSPC data were analyzed with a sliding-scale method (29) to obtain fluorescence lifetime (τ) histograms from recorded photon arrival times. Briefly, the train of photons detected in the FRET donor channel was analyzed in overlapping blocks of 200 consecutive photons, with τ determined for each block by maximum-likelihood estimation (30,31). A histogram of the t_1 arrival times of the photons was used to calculate the likelihood function. The probability distribution for this histogram was approximated by a single exponential decay of the form $e^{-t/\tau}$. Maximizing the logarithm of the likelihood function for the single exponential decay yields

$$\frac{\omega}{1 - e^{-\omega/\tau}} - \frac{T}{e^{T/\tau} - 1} = \frac{\sum_i n_i t_i}{N},$$

where n_i indicates the number of photons in the ith bin of the histogram, and $N = \sum_i n_i$. The value ω is the width of the time bins in the histogram and $t_1 = i\omega$ with $0 \leq t_i \leq T$. The root of this equation yields the maximum-likelihood estimate of the τ-value of the fluorophore for the corresponding t_2 time bracket. The analysis was automated with a custom MATLAB program (The MathWorks, Natick, MA). The method was validated by determining the fluorescence lifetime of Rhodamine 6G in water at room temperature.

FRET efficiency was calculated from measured τ-values according to the relationship $E = (1 - (\tau_{DA}/\tau_D))$, where τ_{DA} values are measurements of two-color SERCA fluorescence lifetime and τ_D is the average τ of the donor-alone control. FRET efficiency histograms were fit to a sum of four Gaussian peaks with the program ORIGIN (OriginLab, Northampton,

MA). All fit parameters (the center value, the width, and the area of each Gaussian) were iteratively varied until convergence was obtained. Parameter mean values were obtained from five independent measurements. In some experiments, background autofluorescence and other light contamination contributes to a long lifetime peak in the lifetime histogram. The lifetime of that species is too long to be from a fluorescent protein tag, so it is disregarded in the FRET analysis.

FRET histogram analysis

Histograms for systole and diastole from the same measurement were globally fit for increased accuracy of the fitted parameters. The center values of the multiple peaks and their widths were shared among these histograms, whereas the areas of the Gaussians were fit independently. Global fitting was also employed in AAV-293 cell measurements by splitting a measurement in time to generate multiple histograms.

Average distances between fluorescent protein fusion tags attached to the N- and A-domains of SERCA were calculated from the center values of sub-populations of the FRET efficiency distributions, and are given in Table 1. Distances are obtained from the relationship $R = R_0(E^{-1} - 1)^{1/6}$, where R_0 is the Förster distance for the FRET pair, and E is the FRET substate peak central value, assuming random relative orientation of the fluorophores ($\kappa^2 = 2/3$). Attachment of the N-terminal fluorescent protein by a flexible linker makes it likely that the probe will sample a wide range of orientations (32) during the dwell time of two-color SERCA in a particular substate. The Förster distance (R_0) is 58.3 Å for the GFP-TagRFP pair and 49.8 Å for the Cer-YFP pair (26). The fluorescent protein FRET pairs for CY-SERCA and RG-SERCA have different R_0, τ_D, and emission spectra. The constructs also have reciprocal donor/acceptor positions. Despite these differences, the distances calculated from FRET substates were very similar for CY-SERCA and RG-SERCA (Table 1). The agreement of these values suggests that the probe separation distance estimate was not dominated by κ^2 or beat-to-beat changes in pH or autofluorescence.

Single molecule time trajectory analysis

FRET efficiency trajectories calculated for each single molecule transit were obtained for analysis of SERCA structural dynamics. FRET efficiency values measured from overlapping blocks of 200 consecutive photons were assigned to specific conformational States I–IV identified from previous Gaussian fitting of FRET efficiency histograms (Table 1). The full width at half-maximum of each Gaussian distribution was used as a threshold for substate assignment. The duration of time spent in each FRET state before transition to another FRET state was quantified, and a histogram of observed dwell times was generated using a custom analysis routine in MATLAB. The histogram of the dwell times was fit by a biexponential function.

TABLE 1 The FRET efficiency of discrete FRET substates and corresponding fluorescent protein chromophore separation distances, obtained from iso-stimulated cardiac myocytes

| State | FRET efficiency | | Probe separation distance (Å) | |
	CY-SERCA	RG-SERCA	CY-SERCA	RG-SERCA
I	−0.004 ± 0.004	0.053 ± 0.002	ND[a]	94.2 ± 0.5
II	0.065 ± 0.004	0.154 ± 0.002	77.8 ± 0.9	77.4 ± 0.2
III	0.120 ± 0.002	0.253 ± 0.002	69.4 ± 0.7	69.8 ± 0.1
IV	0.210 ± 0.006	0.349 ± 0.003	62.1 ± 0.4	64.7 ± 0.2

Distances were calculated using R_0 values of 49.8 Å for CY-SERCA and 58.3 Å for the RG-SERCA. Values are mean ± SE.
[a]Not determined.

RESULTS AND DISCUSSION

FRET in detergent solubilized two-color SERCA

To survey resolvable conformations of SERCA in vitro, we performed pulsed excitation, single-molecule fluorescence spectroscopy with fluorescence lifetime distribution analysis (FLDA) (30,31) using RG-SERCA solubilized in dodecylphosphocholine. Fig. 1 C shows the GFP donor fluorescence emission of RG-SERCA, with bursts of photons indicating the transit through the excitation volume of detergent micelles containing individual two-color SERCA molecules. Fluorescence excited-state lifetimes (τ) were quantified using a sliding-scale analysis method (29). A histogram of measured τ-values revealed a large range of lifetimes from 1.8 to 3.3 ns (Fig. 1 D, *red bars*). The average lifetime was decreased compared to a non-FRET control (donor only) GFP-SERCA (Fig. 1 D, *black striped bars*), consistent with robust intramolecular FRET for RG-SERCA. Moreover, in contrast to the donor-alone τ-distribution, the RG-SERCA histogram exhibited several distinct maxima (Fig. 1 D, *red bars*). The resolved τ-subpopulations suggest at least four discrete FRET states as the proteins diffuse through the excitation volume, consistent with at least four discrete conformations of the pump.

Similar results were obtained for CY-SERCA (see Fig. S1 in the Supporting Material). FRET efficiency histograms for RG-SERCA (Fig. 1 E) or CY-SERCA (Fig. 1 F) were calculated from measured τ-values according to the relationship $E = (1 - (\tau_{DA}/\tau_D))$, where τ_{DA} values are measurements of two-color SERCA fluorescence lifetime and τ_D is the average τ-value of the donor-alone control. The measured donor lifetime for Cer-SERCA control was 2.6 ns (see Fig. S1), slightly less than the published Cer τ-value of 2.99 ns (33). Fusion of Cer to a target protein has been shown to decrease τ-value (33). We obtained a τ-value of 2.86 ns for GFP (Fig. 1 D), which was similar to the published value of 2.96 ns (34). We noted that the discrete subpopulations of two-color SERCA were well resolved, with distributions that were somewhat less wide than the donor only control. One possible explanation for this is that FRET increasingly depletes donors the longer they dwell in the excited state, effectively eroding the right side of the Gaussian and narrowing the width of the lifetime distribution. A four-peak Gaussian fit resolved FRET subpopulations with center values of 0.05, 0.16, 0.25, and 0.34 for RG-SERCA (Fig. 1 E), and −0.01, 0.07, 0.12, and 0.21 for CY-SERCA (Fig. 1 F). A summary of average peak positions is provided in Table 1. We denote these discrete states as I (*orange*), II (*blue*), III (*red*), and IV (*green*), respectively.

The increased FRET efficiency values observed for RG-SERCA substates compared to CY-SERCA are consistent with a longer Förster distance (R_0) for the GFP-TagRFP pair (58.3 Å) versus the Cer-YFP pair (49.8 Å) (26). The apparent separation distances of the fluorescent protein chromophores were calculated according to the Förster relationship (see Supporting Results in the Supporting Material). For CY-SERCA, probe separation distances for States II, III, and IV were 78, 69, and 62 Å, respectively. The FRET efficiency for State I was too low to determine a probe separation distance for this FRET pair. For RG-SERCA, the separation distance for States I, II, III, and IV were 94, 77, 70, and 65 Å, respectively, in good agreement with the measurements made with the Cer-YFP pair (Table 1).

SERCA conformational dynamics

Detergent-solubilized single molecules yielded time-trajectories of up to 800 ms in duration. These showed apparent stochastic transitions between high and low FRET conformations (Fig. 1 G). For comparison, the FRET efficiency of States I–IV identified from the distribution analysis, which is shown in Fig. 1 E, are marked in Fig. 1 G as horizontal lines. The pump was observed to transiently sample the open conformation (State I) before returning to high FRET states during the time trajectories (Fig. 1 G, *arrow*). Such reversibility suggests that the low FRET state does not arise from denatured or proteolyzed two-color SERCA. Analysis of the kinetics of single-molecule structure transitions revealed that SERCA samples States I–IV for variable durations. A histogram of measured substate persistence revealed a biphasic distribution of SERCA dwell times (Fig. 1 H). An exponential fit of this distribution showed the transitions fall into two distinct time regimes. The significance of these two dynamics regimes is not clear. The fast structure fluctuations (80 μs) may represent Brownian dynamics of the N- and A-domains whereas the slower fluctuations (690 μs) may correspond to catalytic transitions between discrete enzymatic substates. Indeed, stochastic thermal fluctuations may power the more deliberate structure transitions of catalysis. The overall rate of transitions increased from 99 ± 55 to 200 ± 61 transitions per minute with the addition of 2 μM Ca.

In general, single-molecule FLDA experiments provided good resolution of discrete FRET states and the transitions between these states. Importantly, because of the small number of molecules sampled, we do not make conclusions about the fractional abundance of particular states in such experiments. The relative population of states was investigated in detail in live cells in experiments described below.

Two-color SERCA expressed in cardiac myocytes

To investigate the structural heterogeneity of SERCA in cardiac muscle, we expressed two-color SERCA in cultured enzymatically isolated rabbit myocytes. We observed a range of expression levels in the population of infected cells. Bright cells were used for confocal imaging of two-color SERCA; for spectroscopy, very dim cells were selected to

reduce the concentration of exogenous protein to minimize the number of fluorescently tagged proteins in the excitation volume. This is a key condition to reduce ensemble averaging and obtain optimal sampling of the distribution of SERCA structural substates. Fig. 2, *A* and *B*, shows confocal fluorescence images of RG-SERCA at 40 h postinfection. Two-color SERCA fluorescence was distributed in striations and longitudinal streaks, suggesting localization in the junctional and transverse sarcoplasmic reticulum, respectively. The localization of RG-SERCA and CY-SERCA (see Fig S2, *A* and *B*) were similar to mCer-SERCA2a localization in adult cardiac myocytes (35). Cardiac myocytes expressing a low concentration of RG-SERCA were selected for FLDA. Ca release and contraction/relaxation were induced by electrical pacing.

Because the τ-value is independent of fluorescence intensity, FLDA measurements were not subject to motion artifacts generated by myocyte contractions. Fig. 2, *C* and *D*, shows examples of FRET efficiency histograms obtained during diastole (relaxation) and systole (contraction), respectively. The distributions were well described by a fit to three Gaussian subpopulations, consistent with three discrete FRET states, corresponding to at least three distinct contemporaneous conformations of SERCA. The parameters of the Gaussian fits were all freely variable, so it is noteworthy that the center FRET efficiency values of the subpopulations closely matched States I, II, and III previously identified in detergent-solubilized SERCA (as in Fig. 1). Interestingly, the high FRET state (IV) observed in single-molecule experiments (Fig. 1, *E* and *F*) was not detected under these conditions; fitting to four Gaussian populations returned zero amplitude for the fourth peak (Fig. 2, *C* and *D*, *green*). The relative population of each state was quantified from the area under the Gaussian for each independent experiment. Combined data are summarized in Fig. 2, *G* and *H*, as mean $\pm$ SE. Overall, the majority of SERCA resided in low FRET states (I and II) during diastole. With the increase in Ca during systole, the population of high FRET State III increased from 12.3 to 34.7% of total (Table 2). Gains in State III came at the expense of the population of low FRET efficiency State I and to a lesser extent, State II (Fig. 2, *G* and *H*, and Table 2).

An alternative analysis examined the time-dependent changes in the populations of SERCA substates with 100-ms time resolution (see Fig. S3). The improved time resolution came at the expense of state discrimination, but despite rather noisy signals, we were able to observe a transient increase in the population of high FRET states after an electrical stimulus (see Fig. S3 *A*, *arrow*), with a concomitant decrease in the relative population of low FRET states (see Fig. S3 *B*). After several hundred milliseconds, the population relaxed again and remained in favor of predominantly low FRET (~80% I and II) for the balance of diastole. Overall, the data suggest that Ca binding to SERCA stabilizes a compact, high FRET structure (III) (Fig. 2 *D*),
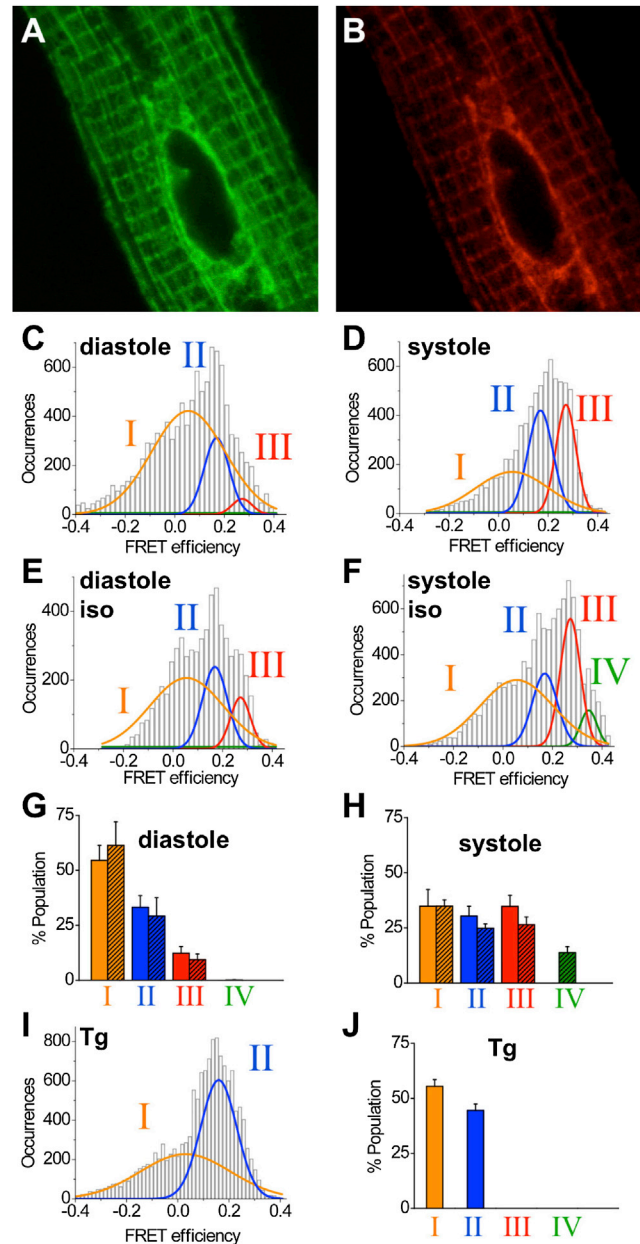

FIGURE 2 Two-color SERCA expressed in adult ventricular cardiac myocytes. (*A*) Localization of RG-SERCA GFP fluorescence in adult ventricular myocytes. (*B*) Localization of RG-SERCA TagRFP fluorescence. (*C*) FRET distribution of two-color SERCA in electrically paced myocytes, during the relaxation phase (diastole). (*D*) Systole (during the contraction phase). (*E*) Diastole, plus isoproterenol. (*F*) Systole, plus isoproterenol. (*G*) Summary of FRET subpopulations during diastole before (*solid bars*) or after addition of isoproterenol (*striped bars*). (*H*) Systole, before (*solid bars*) or after addition of isoproterenol (*striped bars*). (*I*) FRET distribution after addition of Tg. (*J*) Summary of data in panel *I*. Panels *C–F* and *I* are representative data obtained from individual cells; each histogram integrates multiple consecutive contraction/relaxation cycles. Panels *G*, *H*, and *J* are mean $\pm$ SE of all data. To see this figure in color, go online.

consistent with our previous observation that two-color SERCA average FRET increased with Ca ((16) and S. J. Gruber, R. L. Cornea, J. Li, K. C. Peterson, T. M. Schaaf,

TABLE 2 Changes in the relative population of discrete FRET substates in cardiac myocytes, expressed as a percent of total

RG-SERCA FRET substate population (%), in cardiac myocytes

	Control		100 μM Iso		
State	Diastole	Systole	Diastole	Systole	10 μM Tg
I	54.5 ± 6.8	34.9 ± 7.6	61.3 ± 10.7	34.9 ± 2.8^a	55.5 ± 3.0
II	33.2 ± 5.3	30.4 ± 4.5	29.2 ± 8.4	24.9 ± 2.0	44.5 ± 3.0
III	12.3 ± 3.1	34.7 ± 5.0^b	9.4 ± 2.6	26.4 ± 3.5^b	ND[c]
IV	ND[c]	ND[c]	0.1 ± 0.1	13.8 ± 2.8 [b]	ND[c]

Values are mean $\pm$ SE.
[a] $p < 0.05$ versus diastole.
[b] $p < 0.01$ versus diastole.
[c] Not determined.

G. D. Gillispie, R. Dahl, K. M. Zsebo, S. L. Robia, and D. D. Thomas, unpublished).

We also investigated the effect of adrenergic stimulation on SERCA structural heterogeneity. The effect of β-agonist (isoproterenol) was not apparent during diastole, with the majority of SERCA assuming low FRET conformations (States I and II) (Fig. 2 E), similar to untreated myocytes (Fig. 2 C). However, the effect of β-agonist was revealed during systole, with a significant fraction of pumps switching to the latent high FRET state (IV) (Fig. 2 F, Table 2, and see Fig. S2) that was first observed in detergent-solubilized SERCA (Fig. 1, E and F). The observed high FRET efficiency indicates this unique structure is characterized by a very tightly closed cytoplasmic headpiece. One possible interpretation of this result is that the high FRET state results from unbinding of PLB from SERCA (13,36). The alternative interpretation that we prefer is that PLB remains associated with SERCA after phosphorylation, and together with elevated Ca, stabilizes SERCA in a new conformation (37–40). These two alternative mechanisms are directly tested below.

It is interesting that a relatively small fraction of the SERCA population in cultured myocytes switch from the prevailing low FRET states in diastole (Fig. 2, C and E) to high FRET states in systole (Fig. 2, D and F). Indeed, under physiological conditions the population of SERCA is not expected to synchronously transition between various substates en masse. The density of SERCA in the SR is such that each pump would only have to turn over once to completely sequester available Ca (41). The results underscore the value of lifetime distribution analysis for handling structural heterogeneity in the population of proteins. Conventional FRET measurements report the average of all contemporaneous conformations, blurring substates and reducing the apparent magnitude of conformational changes.

Overall, experiments with electrically paced cardiac myocytes suggest that low FRET states (I and II) correspond to Ca-free (E2) conformations whereas high FRET states (III and IV) correspond to Ca-bound conformations. Consistent with this interpretation, Tg treatment abolished states III and IV, leaving SERCA approximately evenly divided between States I and II (Fig. 2, I and J). Tg inhibits SERCA

activity, and is commonly used to lock SERCA into a state that is taken as a surrogate for E2 (21,42). Others have demonstrated that SERCA cytoplasmic domains are still dynamic after Tg binding (43); our data further suggest that Tg-bound SERCA in the E2 enzymatic substate samples at least two discrete conformations.

FRET in two-color SERCA transfected AAV-293 cells

To directly test whether State IV represents a PLB-free SERCA structure or a unique phosphorylated PLB-SERCA regulatory complex conformation, we quantified the distribution of RG-SERCA conformations in AAV-293 cells, which lack endogenous PLB. Confocal microscopy revealed the expected colocalization of the fluorescence of the GFP (Fig. 3 A, green) and TagRFP (Fig. 3 B, red) in internal membrane structures, as was observed previously for CY-SERCA (16), Cer-SERCA (35,44), and CFP SERCA (27,38). The FRET efficiency histogram did not present the high FRET state (IV), whether SERCA was expressed alone (Table 3) or with nonphosphorylatable mutant S16A-PLB (Fig. 3, C and D). Interestingly, coexpression of PLB containing a mutation that mimics phosphorylation by PKA (S16E-PLB) restored the population of State IV, but only in cells that were treated with ionomycin to increase cytosolic Ca (Fig. 3 F) (Table 3). It is not clear why the fourth state, clearly resolved in detergent solution (Fig. 1, E and F), is suppressed in heterologous cells (Fig. 3, C–E) and cardiac myocytes (Fig. 2, C–E). It is also not known why the combination of Ca and PLB phosphorylation uncovers this latent conformation (Figs. 2 F and 3 F).

The data are not consistent with the model in which phosphorylation and Ca relieve SERCA inhibition by dissociating the PLB-SERCA regulatory complex (13,36), because State IV is not observed in the absence of PLB (Table 3). Previously, we (Z. James, J.E. McCaffrey, …, D.D. Thomas. Unpublished) (35,37–38,45) and others (40,46–48) have provided evidence that relief of SERCA inhibition does not require dissociation of PLB. We have proposed that PLB phosphorylation alters the quaternary conformation of the PLB-SERCA complex, without dissociation of the proteins. State IV observed here may correspond to this disinhibited conformation, a unique structure with a very tight headpiece conformation (probe separation distance 62–65 Å). Some reports suggest that phosphorylated PLB provides SERCA with an alternative kinetic pathway (47), enhancing its catalytic efficiency (49–51). The high FRET State IV observed here may represent an activated intermediate substate in this putative alternative pathway.

Magnitude of E2/E1 structure transition

It is noteworthy that there is a 30 Å difference in distance between the most extreme open E2 (I) and closed E1 states
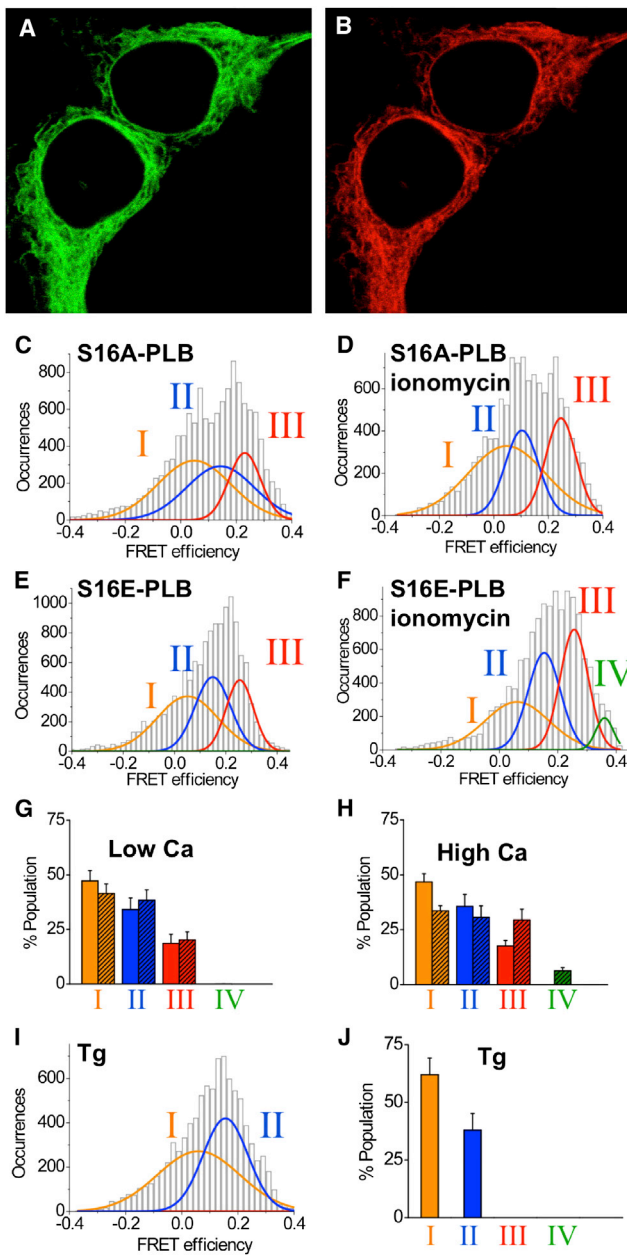
FIGURE 3 Expression of two-color SERCA in AAV-293 cells. (*A*) Localization of RG-SERCA GFP fluorescence in AAV-293 cells. (*B*) Localization of RG-SERCA TagRFP fluorescence. (*C*) FRET distribution of two-color SERCA and nonphosphorylatable PLB in intact cells. (*D*) As in panel *C*, plus ionophore. (*E*) Two-color SERCA plus phosphomimetic PLB. (*F*) As in panel *E*, plus ionophore. (*G*) Summary of FRET subpopulations from intact cells expressing two-color SERCA and nonphosphorylatable PLB (*solid bars*) or phosphomimetic PLB (*striped bars*). (*H*) Plus ionophore, with nonphosphorylatable PLB (*solid bars*) or phosphomimetic PLB (*striped bars*). (*I*) FRET distribution after addition of Tg. (*J*) Summary of *I*. Panels *C*–*F* and *I* are representative data obtained from individual cells. Panels *G*, *H*, and *J* are mean ± SE of all data. To see this figure in color, go online.

(IV) (Table 1). This is a larger difference than would be predicted from x-ray crystal structures. Significant structures (19) from recent x-ray crystallography studies show on

average a ~6 Å difference in the distance between the FRET donor and acceptor fusion sites for E1 structures versus E2 structures. A significant outlier is the first E1 crystal structure 1SU4, characterized by a widely open headpiece structure. It has been proposed that this was an artifact arising from the absence of nucleotide in the crystallization conditions (23,52). Although we did not directly detect an open E1 structure, the presence of a very low FRET E2 state with a 94 Å probe separation distance suggests that the 1SU4 structure represents a real conformation that is significantly populated in vivo (Table 2). We do not think it likely that the low FRET state arises from partially expressed proteins lacking the acceptor fluorophore, because the pump was observed to reversibly sample this state (Fig. 1 *G*). Moreover, State I was observed for both RG-SERCA (Fig. 1 *E*) and CY-SERCA (Fig. 1 *F*), which have a different order of translation of donor and acceptor probes.

Differential disorder of SERCA structures

In addition to revealing the intrinsic FRET efficiency of discrete FRET states, Gaussian fitting also provided estimates of the variability of FRET observed for each state. These parameters are obtained from the peak center position and peak width, respectively. In general, histograms obtained from dilute single molecules in detergent solution were better resolved than those obtained from a higher density of fluorescent molecules in cell membranes. This is consistent with the expected ensemble averaging of multiple molecules diffusing simultaneously through the excitation volume in the cell. However, despite some loss of peak resolution in live cell experiments, we were still able to observe an inverse relationship between Gaussian width and peak center position (Fig. 4 *A*), irrespective of iso or Tg treatment. The data show that as FRET increases, the variability of FRET decreases. CY-SERCA showed the same trend, and the peak widths were similar to those obtained for RG-SERCA, although the reduced Cer-YFP R_0 resulted in correspondingly decreased FRET for each state (Fig. 4 *B*). That the two constructs gave similar peak widths despite different Förster distances supports the conclusion that the Gaussian widths are set by SERCA structural disorder. Specifically, the inverse relationship of peak width and peak center position indicates that the domain separation distance becomes increasingly well defined with closure of the cytoplasmic headpiece.

Overall, the results suggest a high degree of cytoplasmic domain structural disorder for open structures, and a well-defined, rigid architecture for compact structures. It is possible that high-FRET, tightly closed conformations are stabilized by domain-domain contacts, whereas open conformations are unconstrained and floppy. The functional consequence of dynamic open architecture may be enhanced mobility of the nucleotide binding domain during

TABLE 3   Changes in the relative population of discrete FRET substates in AAV-293 cells, expressed as percent of total

RG-SERCA FRET substate population (%), in AAV-293 cells

	S16A-PLB		S16E-PLB			
State	Low Ca	High Ca	Low Ca	High Ca	10 μM Tg	no PLB
I	47.2 ± 4.8	46.8 ± 3.7	41.5 ± 4.4	33.6 ± 2.3	62.0 ± 7.2	12.8 ± 3.7
II	34.1 ± 5.4	35.6 ± 5.5	38.3 ± 4.9	30.6 ± 5.3	38.0 ± 7.2	58.2 ± 12.5
III	18.6 ± 4.1	17.6 ± 2.5	20.2 ± 3.6	29.4 ± 5.0	ND[a]	28.2 ± 12.0
IV	ND[a]	ND[a]	ND[a]	6.3 ± 1.5	ND[a]	ND[a]

Values are mean ± SE.

[a]Not determined.

its Brownian search for ATP substrate. We have previously proposed that Ca-free (E2) SERCA can assume an open headpiece conformation ([16]). This hypothesis is compatible with our data. Specifically, we observe several dynamic, low FRET structures in low Ca (States I and II), and these struc-
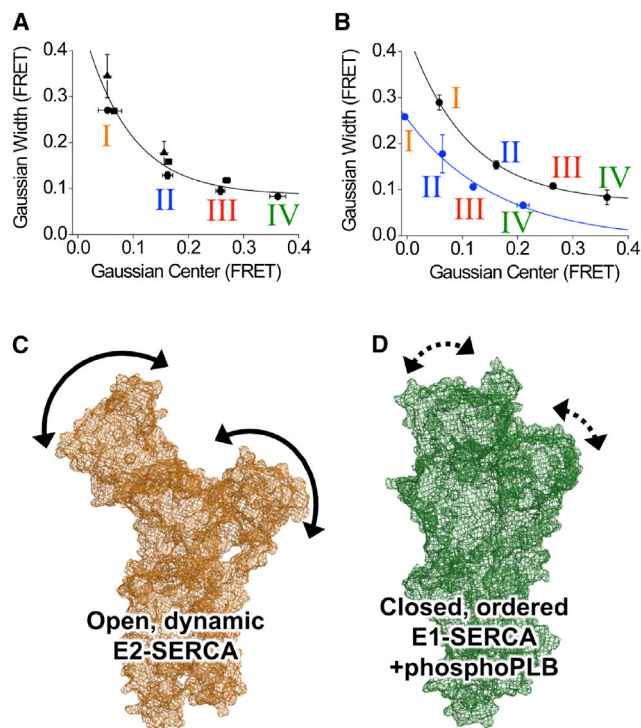

FIGURE 4   Comparison of FRET histogram Gaussian fit width versus center position data obtained from cardiac myocytes. (A) States I–IV for RG-SERCA showed that the population Gaussian width decreased with increasing population Gaussian center value. This relationship was not detectably altered by Tg (*triangles*) or iso (*squares*) compared to control (*circles*). The data suggest that low FRET (*open*) conformations are more dynamically disordered than high FRET (*solid*) structures. (B) Average RG-SERCA peak parameters (*black*) compared with CY-SERCA (*blue*). The shorter R_0 of the Cer/YFP pair yielded decreased FRET (*decreased center values*), but similar Gaussian widths for each state. Data are mean ± SE. Proposed novel conformation of SERCA: (C) open E2 (Ca-free) SERCA, characterized by a dynamically disordered cytoplasmic headpiece; and (D) proposed closed E1 (Ca-bound) SERCA, with a rigidly ordered headpiece. The conformation represents a unique E1 state that is stabilized by phosphorylated phospholamban. To see this figure in color, go online.

tures are stabilized by Tg. We did not resolve any new peaks after Tg addition, consistent with the recent crystallographic study showing that Tg stabilizes an existing E2 state without distorting ATPase structure ([53]). During the preparation of this manuscript, Akin et al. reported a crystal structure of Ca-free SERCA bound to PLB, which showed an open cytoplasmic headpiece ([54]). We consider that structure to be compatible with our present evidences for a dynamic open E2. Conversely, the compact and ordered structure of State IV (E1-SERCA bound to phosphorylated PLB) makes it an interesting candidate for high-resolution structure studies. Previously, cocrystallization studies have focused on capturing the regulatory complex of PLB with E2-SERCA ([54–56]).

Recently, several groups successfully obtained high-resolution structures of sarcolipin bound to SERCA in an Mg-bound E1 state ([53,57]). Sarcolipin is a peptide regulator analogous to PLB, and has been shown to remain bound to SERCA in the presence and absence of Ca ([14,53,58]). We take this as consistent with our contention that regulatory partners may interact with both E1 and E2-SERCA ([45]), albeit with decreased affinity ([35]). We have speculated that the PLB-E1-SERCA binding interface is distinct from the canonical M2/M6/M9 binding groove on E2-SERCA ([35]). This may be why PLB-SERCA cross-linking is reduced ([53]) or abolished ([13,14,54,58]) by Ca while SERCA-PLB FRET is preserved.

CONCLUSIONS

We have determined that the new FRET construct RG-SERCA was properly localized, functional, and responsive to conformational changes. Reversible transitions among four discrete conformations are consistent with fast (80-μs) Brownian motions and slow (690-μs) catalytic motions. These are large-amplitude transitions, producing a ~30 Å change in FRET pair separation distance. Low FRET states are consistent with open, dynamic structures, and prevail in the low Ca conditions that favor the SERCA E2 enzymatic substate. High Ca, which favors the SERCA E1 substate, stabilizes high FRET states, with closed, rigidly ordered cytoplasmic headpiece conformations. The data are consistent with our previous conclusion

that the SERCA cytoplasmic headpiece closes with Ca-binding (16).

Significantly, in all conditions we observed considerable heterogeneity. In particular, although we predicted SERCA inhibition would lock the pump into a single conformation and simplify the FRET histogram to a single peak, multiple discrete conformations were still present after addition of Tg. The inhibitor eliminated two of the substates, but two remain, and we observed reversible transitions of the inhibited pump between these discrete states. Such heterogeneity was not predicted by the many Tg-bound structures available in the literature. Thus, apparently homogenous subconformations of SERCA, such as obtained in x-ray crystallography, may not represent the true dynamic structure of the ATPase. Instead, presumed enzymatic substates may actually be an ensemble of degenerate conformations.

Consistent with our previous studies, phosphorylation of phospholamban did not dissociate it from SERCA (38), nor does Ca-binding to SERCA abolish the regulatory complex (35). Instead, Ca-binding to SERCA and phospholamban phosphorylation together induce the SERCA cytoplasmic headpiece to sample a unique high FRET conformation. Taken together, the results predict several novel states that are not represented in the available x-ray crystal structures: an E2 state with a dynamically disordered open cytoplasmic headpiece (Fig. 4C), and a tightly closed E1-Ca-SERCA bound to phosphorylated PLB (Fig.4D).

SUPPORTING MATERIAL

REFERENCES

1. Periasamy, M., and S. Huke. 2001. SERCA pump level is a critical determinant of Ca^{2+} homeostasis and cardiac contractility. *J. Mol. Cell. Cardiol.* 33:1053–1063.

2. Wold, L. E., K. Dutta, …, A. J. Davidoff. 2005. Impaired SERCA function contributes to cardiomyocyte dysfunction in insulin resistant rats. *J. Mol. Cell. Cardiol.* 39:297–307.

3. Haghighi, K., F. Kolokathis, …, E. G. Kranias. 2006. A mutation in the human phospholamban gene, deleting arginine 14, results in lethal, hereditary cardiomyopathy. *Proc. Natl. Acad. Sci. USA.* 103:1388–1393.

4. Haghighi, K., F. Kolokathis, …, E. G. Kranias. 2003. Human phospholamban null results in lethal dilated cardiomyopathy revealing a critical difference between mouse and human. *J. Clin. Invest.* 111:869–876.

5. Schmitt, J. P., M. Kamisago, …, C. E. Seidman. 2003. Dilated cardiomyopathy and heart failure caused by a mutation in phospholamban. *Science.* 299:1410–1413.

6. Bigelow, D. J., and G. Inesi. 1992. Contributions of chemical derivatization and spectroscopic studies to the characterization of the Ca^{2+} transport ATPase of sarcoplasmic reticulum. *Biochim. Biophys. Acta.* 1113:323–338.

7. Autry, J. M., J. E. Rubin, …, D. D. Thomas. 2012. Nucleotide activation of the Ca-ATPase. *J. Biol. Chem.* 287:39070–39082.

8. Inesi, G., D. Lewis, …, L. de Meis. 2008. Conformational fluctuations of the Ca^{2+}-ATPase in the native membrane environment. Effects of pH, temperature, catalytic substrates, and thapsigargin. *J. Biol. Chem.* 283:1189–1196.

9. Mueller, B., M. Zhao, …, D. D. Thomas. 2004. SERCA structural dynamics induced by ATP and calcium. *Biochemistry.* 43:12846–12854.

10. Espinoza-Fonseca, L. M., and D. D. Thomas. 2011. Atomic-level characterization of the activation mechanism of SERCA by calcium. *PLoS ONE.* 6:e26936.

11. Kekenes-Huskey, P. M., V. T. Metzger, …, J. A. McCammon. 2012. Calcium binding and allosteric signaling mechanisms for the sarcoplasmic reticulum Ca^{2+} ATPase. *Protein Sci.* 21:1429–1443.

12. Akin, B. L., Z. Chen, and L. R. Jones. 2010. Superinhibitory phospholamban mutants compete with Ca^{2+} for binding to SERCA2a by stabilizing a unique nucleotide-dependent conformational state. *J. Biol. Chem.* 285:28540–28552.

13. Chen, Z., B. L. Akin, and L. R. Jones. 2010. Ca^{2+} binding to site I of the cardiac Ca^{2+} pump is sufficient to dissociate phospholamban. *J. Biol. Chem.* 285:3253–3260.

14. Sahoo, S. K., S. A. Shaikh, …, M. Periasamy. 2013. Sarcolipin protein interaction with sarco(endo)plasmic reticulum Ca^{2+} ATPase (SERCA) is distinct from phospholamban protein, and only sarcolipin can promote uncoupling of the SERCA pump. *J. Biol. Chem.* 288:6881–6889.

15. Corradi, G. R., and H. P. Adamo. 2007. Intramolecular fluorescence resonance energy transfer between fused autofluorescent proteins reveals rearrangements of the N- and C-terminal segments of the plasma membrane Ca^{2+} pump involved in the activation. *J. Biol. Chem.* 282:35440–35448.

16. Hou, Z., Z. Hu, …, S. L. Robia. 2012. 2-Color calcium pump reveals closure of the cytoplasmic headpiece with calcium binding. *PLoS ONE.* 7:e40369.

17. Satoh, K., T. Matsu-Ura, …, K. Mikoshiba. 2011. Highly cooperative dependence of sarco/endoplasmic reticulum calcium ATPase SERCA2a pump activity on cytosolic calcium in living cells. *J. Biol. Chem.* 286:20591–20599.

18. Winters, D. L., J. M. Autry, …, D. D. Thomas. 2008. Interdomain fluorescence resonance energy transfer in SERCA probed by cyan-fluorescent protein fused to the actuator domain. *Biochemistry.* 47:4246–4256.

19. Møller, J. V., C. Olesen, …, P. Nissen. 2010. The sarcoplasmic Ca^{2+}-ATPase: design of a perfect chemi-osmotic pump. *Q. Rev. Biophys.* 43:501–566.

20. Toyoshima, C., M. Nakasako, …, H. Ogawa. 2000. Crystal structure of the calcium pump of sarcoplasmic reticulum at 2.6 Å resolution. *Nature.* 405:647–655.

21. Toyoshima, C., and H. Nomura. 2002. Structural changes in the calcium pump accompanying the dissociation of calcium. *Nature.* 418:605–611.

22. Olesen, C., T. L. Sørensen, …, P. Nissen. 2004. Dephosphorylation of the calcium pump coupled to counterion occlusion. *Science.* 306:2251–2255.

23. Sørensen, T. L., J. V. Møller, and P. Nissen. 2004. Phosphoryl transfer and calcium ion occlusion in the calcium pump. *Science.* 304:1672–1675.

24. Toyoshima, C., H. Nomura, and T. Tsuda. 2004. Lumenal gating mechanism revealed in calcium pump crystal structures with phosphate analogues. *Nature.* 432:361–368.

25. Reference deleted in proof.

26. Gadella, T. W. J. 2009. FRET and FLIM Techniques. Elsevier, Amsterdam, Netherlands.

27. Kelly, E. M., Z. Hou, …, S. L. Robia. 2008. Phospholamban oligomerization, quaternary structure, and sarco(endo)plasmic reticulum calcium ATPase binding measured by fluorescence resonance energy transfer in living cells. *J. Biol. Chem.* 283:12202–12211.

28. Domeier, T. L., L. A. Blatter, and A. V. Zima. 2009. Alteration of sarcoplasmic reticulum Ca^{2+} release termination by ryanodine receptor sensitization and in heart failure. *J. Physiol.* 587:5197–5209.

29. Eggeling, C., J. R. Fries, …, C. A. Seidel. 1998. Monitoring conformational dynamics of a single molecule by selective fluorescence spectroscopy. *Proc. Natl. Acad. Sci. USA.* 95:1556–1561.

30. Bajzer, Ž., T. M. Therneau, …, F. G. Prendergast. 1991. Maximum likelihood method for the analysis of time-resolved fluorescence decay curves. *Eur. Biophys. J.* 20:247–262.

31. Maus, M., M. Cotlet, …, C. A. Seidel. 2001. An experimental comparison of the maximum likelihood estimation and nonlinear least-squares fluorescence lifetime analysis of single molecules. *Anal. Chem.* 73:2078–2086.

32. dos Remedios, C. G., and P. D. Moens. 1995. Fluorescence resonance energy transfer spectroscopy is a reliable "ruler" for measuring structural changes in proteins. Dispelling the problem of the unknown orientation factor. *J. Struct. Biol.* 115:175–185.

33. Koushik, S. V., and S. S. Vogel. 2008. Energy migration alters the fluorescence lifetime of Cerulean: implications for fluorescence lifetime imaging Forster resonance energy transfer measurements. *J. Biomed. Opt.* 13:031204.

34. Volkmer, A., V. Subramaniam, …, T. M. Jovin. 2000. One- and two-photon excited fluorescence lifetimes and anisotropy decays of green fluorescent proteins. *Biophys. J.* 78:1589–1598.

35. Bidwell, P., D. J. Blackwell, …, S. L. Robia. 2011. Phospholamban binds with differential affinity to calcium pump conformers. *J. Biol. Chem.* 286:35044–35050.

36. Asahi, M., E. McKenna, …, D. H. MacLennan. 2000. Physical interactions between phospholamban and sarco(endo)plasmic reticulum Ca^{2+}-ATPases are dissociated by elevated Ca^{2+}, but not by phospholamban phosphorylation, vanadate, or thapsigargin, and are enhanced by ATP. *J. Biol. Chem.* 275:15034–15038.

37. Gruber, S. J., S. Haydon, and D. D. Thomas. 2012. Phospholamban mutants compete with wild type for SERCA binding in living cells. *Biochem. Biophys. Res. Commun.* 420:236–240.

38. Hou, Z., E. M. Kelly, and S. L. Robia. 2008. Phosphomimetic mutations increase phospholamban oligomerization and alter the structure of its regulatory complex. *J. Biol. Chem.* 283:28996–29003.

39. Reference deleted in proof.

40. Negash, S., L. T. Chen, …, T. C. Squier. 1996. Phosphorylation of phospholamban by cAMP-dependent protein kinase enhances interactions between Ca-ATPase polypeptide chains in cardiac sarcoplasmic reticulum membranes. *Biochemistry.* 35:11247–11259.

41. Hove-Madsen, L., and D. M. Bers. 1993. Sarcoplasmic reticulum Ca^{2+} uptake and thapsigargin sensitivity in permeabilized rabbit and rat ventricular myocytes. *Circ. Res.* 73:820–828.

42. Paula, S., and W. J. Ball, Jr. 2004. Molecular determinants of thapsigargin binding by SERCA Ca^{2+}-ATPase: a computational docking study. *Proteins.* 56:595–606.

43. Montigny, C., M. Picard, …, P. Champeil. 2007. Inhibitors bound to Ca^{2+}-free sarcoplasmic reticulum Ca^{2+}-ATPase lock its transmembrane region but not necessarily its cytosolic region, revealing the flexibility of the loops connecting transmembrane and cytosolic domains. *Biochemistry.* 46:15162–15174.

44. Hou, Z., and S. L. Robia. 2010. Relative affinity of calcium pump isoforms for phospholamban quantified by fluorescence resonance energy transfer. *J. Mol. Biol.* 402:210–216.

45. Mueller, B., C. B. Karim, …, D. D. Thomas. 2004. Direct detection of phospholamban and sarcoplasmic reticulum Ca-ATPase interaction in membranes using fluorescence resonance energy transfer. *Biochemistry.* 43:8754–8765.

46. Bigelow, D. J., T. C. Squier, and G. Inesi. 1992. Phosphorylation-dependent changes in the spatial relationship between Ca-ATPase polypeptide chains in sarcoplasmic reticulum membranes. *J. Biol. Chem.* 267:6952–6962.

47. Mahaney, J. E., R. W. Albers, …, J. P. Froehlich. 2005. Intermolecular conformational coupling and free energy exchange enhance the catalytic efficiency of cardiac muscle SERCA2a following the relief of phospholamban inhibition. *Biochemistry.* 44:7713–7724.

48. Negash, S., Q. Yao, …, T. C. Squier. 2000. Phospholamban remains associated with the Ca^{2+}- and Mg^{2+}-dependent ATPase following phosphorylation by cAMP-dependent protein kinase. *Biochem. J.* 351:195–205.

49. Frank, K., C. Tilgmann, …, E. G. Kranias. 2000. Regulatory role of phospholamban in the efficiency of cardiac sarcoplasmic reticulum Ca^{2+} transport. *Biochemistry.* 39:14176–14182.

50. Shannon, T. R., G. Chu, …, D. M. Bers. 2001. Phospholamban decreases the energetic efficiency of the sarcoplasmic reticulum Ca pump. *J. Biol. Chem.* 276:7195–7201.

51. Antipenko, A. Y., A. I. Spielman, …, M. A. Kirchberger. 1997. Comparison of the kinetic effects of phospholamban phosphorylation and anti-phospholamban monoclonal antibody on the calcium pump in purified cardiac sarcoplasmic reticulum membranes. *Biochemistry.* 36:12903–12910.

52. Jensen, A. M., T. L. Sørensen, …, P. Nissen. 2006. Modulatory and catalytic modes of ATP binding by the calcium pump. *EMBO J.* 25:2305–2314.

53. Toyoshima, C., S. Iwasawa, …, G. Inesi. 2013. Crystal structures of the calcium pump and sarcolipin in the Mg^{2+}-bound E1 state. *Nature.* 495:260–264.

54. Akin, B. L., T. D. Hurley, …, L. R. Jones. 2013. The structural basis for phospholamban inhibition of the calcium pump in sarcoplasmic reticulum. *J. Biol. Chem.* 2013 Aug 31. [Epub ahead of print].

55. Glaves, J. P., C. A. Trieber, …, H. S. Young. 2011. Phosphorylation and mutation of phospholamban alter physical interactions with the sarcoplasmic reticulum calcium pump. *J. Mol. Biol.* 405:707–723.

56. Young, H. S., L. R. Jones, and D. L. Stokes. 2001. Locating phospholamban in co-crystals with Ca^{2+}-ATPase by cryoelectron microscopy. *Biophys. J.* 81:884–894.

57. Winther, A. M., M. Bublitz, …, M. J. Buch-Pedersen. 2013. The sarcolipin-bound calcium pump stabilizes calcium sites exposed to the cytoplasm. *Nature.* 495:265–269.

58. Bal, N. C., S. K. Maurya, …, M. Periasamy. 2012. Sarcolipin is a newly identified regulator of muscle-based thermogenesis in mammals. *Nat. Med.* 18:1575–1579.